Lab on a Chip

Accepted Manuscript

ROYAL SOCIETY OF CHEMISTRY

www.rsc.org/loc

Magnetic Steering Control of Multi-Cellular Bio-Hybrid Microswimmers

Rika Wright Carlsen[¥], Matthew R. Edwards[¥], Jiang Zhuang, Cecile Pacoret, and Metin Sitti[*,§]

Department of Mechanical Engineering, Carnegie Mellon University, Pittsburgh, Pennsylvania 15213, USA

[¥] Equally contributing authors
[§] Also, Max Planck Institute for Intelligent Systems, 70569 Stuttgart, Germany
[*] Corresponding author: sitti@cmu.edu

Keywords: Bio-hybrid, microswimmer, magnetic steering, microrobot, bacteria

Bio-hybrid devices, which integrate biological cells with synthetic components, have opened a new path in miniaturized systems with the potential to provide actuation and control for systems down to a few microns in size. Here, we address the challenge of remotely controlling bio-hybrid microswimmers propelled by multiple bacterial cells. These devices have been proposed as a viable method for targeted drug delivery but have also been shown to exhibit stochastic motion. We demonstrate a method of remote magnetic control that significantly reduces the stochasticity of the motion, enabling steering control. The demonstrated microswimmers consist of multiple *Serratia marcescens* (*S. marcescens*) bacteria attached to a 6 μm-diameter superparamagnetic bead. We characterize their motion and define the parameters governing their controllability. We show that the microswimmers can be controlled along two-dimensional (2-D) trajectories using weak magnetic fields (≤ 10 mT) and can achieve 2-D swimming speeds up to 7.3 μm/s. This magnetic steering approach can be integrated with sensory-based steering in future work, enabling new control strategies for bio-hybrid microsystems.

Introduction

Bio-hybrid propulsion has proven to be an effective method of untethered actuation of microdevices.[1-3] This strategy employs contractile or motile biological cells as on-board actuators and has led to novel microsystems, such as microwalkers and microswimmers actuated by contractile cardiomyocytes[4-7] and microswimmers actuated by the rotating flagella of bacteria.[8-19] Living cells have a unique advantage over other actuators in that they can also serve as on-board sensors due to their intrinsic sensing ability. Control strategies that utilize the cell's sensory and behavioral response to environmental stimuli, such as to chemical, light, pH and temperature gradients, have been explored.[20] It is an attractive approach for applications that have strong environmental cues that can elicit a bacterial response, such as biochemical signals in targeted drug delivery.[21] However, these control methods cannot be used in homogeneous environments where there may not be a strong behavioral response. Furthermore, sensory-based methods have limited steering controllability. For example, directional motion of bacteria-propelled microdevices along chemical gradients has been demonstrated; however, a strong stochastic contribution to the motion still remains, reducing the precision of the control.[15,18,22,23] As a result, externally driven control strategies that do not rely on cellular sensing must be explored to improve the steering control of bio-hybrid microdevices. Here, we demonstrate a method of remote magnetic control that significantly reduces the stochasticity of motion and enables directional control of the microdevices.

The use of magnetic fields is an attractive option for microsystem steering because the fields can be generated remotely and can penetrate most environments, such as the human body and lab-on-a-chip devices.[2] Magnetic steering control has been successfully applied to non-biological microdevices.[24-34] These devices do not have on-board actuators and require

applied magnetic forces, rotating magnetic fields, or chemical reactions for propulsion. In contrast to bio-hybrid approaches, non-biological microdevices often do not have integrated on-board sensors and thus cannot respond to environmental stimuli.

By integrating magnetic steering with bio-hybrid propulsion, remote actuation and both externally driven and sensory-based steering can be achieved. Despite the advantages of such an approach, few studies have investigated the integration of these two methods. The primary approach to magnetically steer a bio-hybrid microdevice has been to use biological components that are sensitive to magnetic fields, such as magnetotactic bacteria, or cells with embedded magnetic particles.[11,35-40] These methods rely on cells with a magnetic sensing capability or on cells that can remain viable after the incorporation of magnetic nanoparticles, limiting the type of cells that can be applied. Recently, Magdanz *et al.* demonstrated the magnetic steering control of a micro-tube actuated by a single spermatozoid, showing for the first time the integration of magnetic steering with a bio-hybrid device propelled by a non-magnetic biological cell.[41] The approach requires the cell to be oriented with the axis of the magnetic micro-tube, which is achieved by trapping the cell inside the tube.

Here, we demonstrate that magnetic steering can be applied towards the directional control of microdevices propelled by multiple bacterial cells without strictly aligning the cells on the device. Bacteria-driven microswimmers have received much attention as a potential carrier of therapeutic agents in targeted drug delivery applications;[20,21] however, precise steering control of these heterogeneous systems has proven to be a challenge since there is a strong stochastic contribution to their motion. With the proposed magnetic steering method, the stochasticity of the motion can be significantly reduced. We analyze the one-dimensional and two-dimensional steering capabilities of these bio-hybrid microswimmers to better

understand the mechanisms driving their controllability. Based on this analysis, we propose methods for optimizing the steering control. This work is a critical step towards developing future control strategies that utilize both externally-driven and sensory-based steering mechanisms, expanding the potential applications of these devices.

Materials and methods

The bio-hybird microswimmers are fabricated by the spontaneous attachment of one to ten *S. marcescens* cells to a 6 μm-diameter superparamagnetic bead. Although *S. marcescens* is considered pathogenic and cannot be applied to *in vivo* applications without genetic modification, it has been used widely in bio-hybrid microsystems since it is easily cultivated and attaches well to surfaces due to its cell surface hydrophobicity and positive surface charge.[42-44] Given the large number of bio-hybrid microdevices which have already been demonstrated with *S. marcescens*[8,9,12-19,45,46] and the detailed physical information available on the bacteria,[47] we have chosen to use the bacterium to demonstrate the feasibility of our active steering methodology.

Cell preparation

Serratia marcescens (ATCC 274, American Type Culture Collection, Manassas, VA) was cultured to exponential growth phase in liquid nutrient broth (25 g Difco LB Miller Broth and 1 L deionized water, pH 7.0) by incubating on a shaker at 37°C for about 3.5 - 4 hours. The liquid culture was diluted 1:10 in motility medium (0.01 M KH_2PO_4, 0.067M NaCl, 10^{-4} M EDTA, 0.01M glucose, pH = 7.0) before attaching the bacteria to the beads.

Bio-hybrid microswimmer fabrication

The bacteria were attached to 6 μm-diameter streptavidin-coated magnetic beads (COMPEL, Bangs Laboratories, Inc.) through streptavidin-biotin binding. The streptavidin-coated beads were first washed in DI water. Then, 50 μl of the bead solution was added to 200 μl of DI water containing 3 mg of dissolved biotin (Sulfo-NHS-LC-Biotin, BR110, Campbell Science, Rockford, IL). The solution was incubated at room temperature for 45 minutes to allow for biotin-streptavidin binding. The biotin was washed from the bead solution, and the beads were re-suspended in 250 μl of motility medium. Aliquots of the biotin-streptavidin coated magnetic beads (10 μl), the diluted L-broth culture (20 μl), and motility medium (30 μl) were gently mixed and incubated at room temperature for 5 minutes to allow for bacterial attachment to the beads through surface protein binding to the biotin-streptavidin bead coating. After the bacterial attachment, 140 μl of Percoll (Sigma-Aldrich, St. Louis, MO) was added to the solution to increase the fluid density to about 1090 kg/m^3, thereby making the microbeads neutrally buoyant. The final solution was placed in a 5 mm x 5 mm x 2 mm chamber constructed from a polydimethylsiloxane square frame sandwiched between two glass coverslips.

The above fabrication approach can be applied to other similarly sized flagellated bacteria cells, enabling substitution of a suitable bacterial species for a given application. For example, the swimming behavior of *Escherichia coli* (*E. coli*) has been shown to be similar to *S. marcescens*,[47] and *E. coli* could serve as the bioactuator in these devices by biotinylating the cell's surface proteins either through chemical or enzymatic means. The simple fabrication process enables the mass production of hundreds of microswimmers simultaneously. Each bacterium supplies a propulsive force of about 0.5 pN through the

rotation of its flagella.[9,45] By attaching multiple bacteria, it is possible to increase the net propulsive force acting on the bead, allowing the microdevice to carry a larger payload.[48]

Imaging and speed analysis

The bacteria-propelled microbeads were imaged far from the chamber walls at 20 frames per second (QICAM, QImaging) using a 32x objective in an inverted phase contrast microscope (Zeiss Axio Observer). All experiments were conducted at room temperature (21˚C). The images were post-processed using an in-house MATLAB (Mathworks, Natick, MA) script to obtain the bead trajectories. The *x* and *y* bead positions were found using a Hough transform algorithm as described in Edwards *et al.*[9] Given the long acquisition times and computational cost, 3-D tracking was not conducted on all the trajectories. A few trajectories were analyzed with optical 3-D tracking, as described in Edwards *et al.,* to verify the helical nature of the paths.[9] The trajectories were adjusted for any background fluid flow by subtracting the displacements caused by fluid drift from the bead displacements. The fluid drift velocity was computed from the average velocity of all non-motile bacteria (typically around 6 - 10) appearing in each frame. The instantaneous 2-D speeds were measured by first smoothing each trajectory using a five frame moving average and then computing the speeds from adjacent frames of the smoothed trajectory.

Magnetic coil system

Uniform magnetic fields were generated using a magnetic coil system consisting of four iron-core electromagnets oriented 90 degrees from each other (Figure 1). The coils were built onto a microscope stage insert so that it could be placed into an inverted microscope. The coil current was controlled with an Arduino Uno microcontroller board (http://www.arduino.cc), and the magnetic field strength was calibrated using a gauss meter probe (Model 410, Lake

Shore Cryotronics, Inc.). Magnetic field strengths up to 10 mT were used to steer the microrobots.

Statistical methods

The confidence interval for the percent change in the instantaneous speed of the microswimmers before and after the application of the magnetic field (see the section on the one-dimensional steering control) was determined from a sample size of 30 ($N = 30$) using a two-sided Student's t-test with a 95% confidence level. The binomial proportion confidence intervals for the turn success rates (Figure 6a) were statistically assessed from a sample size of 40 ($N = 40$) using a Wilson score interval with a 95% confidence level.[49]

Results

Model of microswimmer motion under a constant magnetic field

The microswimmers were steered in 2-D by varying the direction of a uniform magnetic field **B** produced by two orthogonal electromagnet pairs. The generated magnetic field gradients were negligible in our system; therefore, the translation of the microbead was a result of bacterial propulsion and not due to a magnetic force produced by a field gradient. Steering control required the application of a magnetic torque on the microbeads. Here, we describe how this torque was produced and develop a simple model of the microswimmer motion.

Although the magnetic behavior of the beads is predominately superparamagnetic, there is a slight magnetic anisotropy, which results in the bead having a preferred magnetization direction, called the easy axis.[50-52] Due to this magnetic anisotropy, the bead will tend to physically align its easy axis to an applied magnetic field as shown in Figure 2a.

Upon application of a magnetic field, both the magnetization parallel to the applied field and the magnetization along the easy axis contribute to the effective magnetic moment, **m**, of the bead. The magnetic torque, $\boldsymbol{\tau}_m$, arises from the vector product of the latter with the applied field and can be described as

$$\boldsymbol{\tau}_m = \mathbf{m}_{\parallel} \times \mathbf{B} = \alpha \frac{\chi_b V_b}{\mu_0} |\mathbf{B}| \cos(\phi) \mathbf{e}_{\parallel} \times \mathbf{B} = \alpha \frac{\chi_b V_b}{2\mu_0} |\mathbf{B}|^2 \sin(2\phi) \mathbf{e}_z \qquad (1)$$

where $\mathbf{m}_{\parallel}$ is the component of the magnetic moment along the easy axis, V_b is the bead volume, χ_b is the bead's magnetic susceptibility, μ_0 is the magnetic permeability in a vacuum, α is an anisotropy constant, $\mathbf{e}_{\parallel}$ is a vector denoting the easy axis, and ϕ is the angle between $\mathbf{e}_{\parallel}$ and **B**.[52] Here, we assume that the applied field is lower than the field that saturates the magnetization of the bead. The magnetic susceptibility of our beads was measured to be 0.20 ± 0.05 (95% confidence interval) with a SQUID (superconducting quantum interference device) magnetometer (see Supplementary Fig. 1). Given that the anisotropy constant of superparamagnetic beads is typically around a few percent,[52] the maximum magnetic torque that can be generated for an applied magnetic field of 10 mT is 27 – 45 pN μm (α = 3 – 5%, ϕ = 45°). In comparison, Edwards et al. concluded that a single *S. marcescens* bacterium can produce a propulsive torque, τ_p, of about 4.5 pN μm through the rotation of their flagella.[9] Since the bacterial propulsive torque is an order of magnitude lower than the magnetic torque, we can assume that the magnetic torque is dominant ($\tau_m \gg \tau_p$) for a small number of attached bacteria, and the easy axis of the bead will tend to align with the direction of an applied magnetic field for B = 10 mT.

The microswimmer motion may be largely described by a simple model that neglects the intricacies of the flagella-fluid interaction. The bacteria exert a propulsive force $\mathbf{F}_p$, which can be divided into mean $\bar{\mathbf{F}}_p$ and fluctuating $\mathbf{F}'_p$ components (in the bead reference frame),

$$\mathbf{F}_p = \bar{\mathbf{F}}_p + \boldsymbol{F}'_p \qquad (2)$$

as well as a propulsive torque,[9] which can be similarly divided

$$\boldsymbol{\tau}_p = \bar{\boldsymbol{\tau}}_p + \boldsymbol{\tau}'_p \qquad (3)$$

where the fluctuating components average to zero. The propulsive torque is caused by the rotation of the flagella with respect to the cell's body as well as any applied propulsive force off-axis from the bead's center of pressure. The components of the propulsive forces and torques are shown in Figure 2b. These components are defined in terms of those that are parallel to the easy axis of the bead ($\mathbf{F}_p^{\parallel}$ and $\boldsymbol{\tau}_p^{\parallel}$) and those that perpendicular to the easy axis ($\mathbf{F}_p^{\perp}$ and $\boldsymbol{\tau}_p^{\perp}$). The beads swim at low Reynolds number (Re $\approx 3 \times 10^{-5}$), so the fluid drag force and torque from Stoke's law ($\mathbf{F}_d = 6\pi\mu R_b\mathbf{v}$ and $\boldsymbol{\tau}_d = 8\pi\mu R_b^3\boldsymbol{\omega}$) immediately balance the applied forces and torques.

Following the initial re-orientation of the bead upon the application of the field, the magnetic moment and field are considered parallel at all times as shown in Figure 2c. The bead is free to rotate about the magnetic moment axis (i.e. the easy axis); however, any rotation perpendicular to this axis is restricted by the magnetic torque, which forces the magnetic moment to be aligned with the field. As a result, $\boldsymbol{\tau}_p^{\perp}$ is neglected in the model, and only $\boldsymbol{\tau}_p^{\parallel}$ is considered, which induces rotation of the bead about the easy axis (see Figure 2c). Controllability is reduced when this assumption does not hold.

The relationship between $\mathbf{B}$, $\mathbf{F}_p$, and $\boldsymbol{\tau}_p$ as a function of time dictates the microswimmer's motion. To create persistent bias parallel or anti-parallel to the field, the components of the propulsive force and torque parallel to the magnetic field must be non-zero, and the bead must continuously rotate about the magnet moment axis $\left(\bar{\tau}_p^{\parallel} \neq 0\right)$ so that any force component perpendicular to the field will average to zero. If $\bar{\tau}_p^{\parallel}$ is exactly zero,

persistent motion in an arbitrary direction will result. In practice, beads with $\bar{\tau}_p^{\parallel} = 0$ are extremely unlikely since the orientation and distribution of bacteria on the bead are highly random, and there will always be a torque due to the rotation of the flagella. As a result, we can neglect the possibility.

Although most of the beads with a random attachment of bacteria will show biased motion parallel to the direction of an applied field, practical control has more stringent requirements. In qualitative terms, we want the velocity component in the commanded direction ($\mathbf{v}^{\parallel}$) to be as large in magnitude as possible, and the perpendicular component of the velocity ($\mathbf{v}^{\perp}$) to average to zero on a short time scale. From these conditions, restrictions on the propulsive forces and torques follow as listed in Table 1, where F_{other} includes all other forces in the system (e.g. buoyancy, Brownian forces, etc.). For example, the fluctuations in the propulsive force and torque should be small. The maximum magnetic torque should be greater than $\tau_p^{\perp}$, and the propulsive force in the commanded direction should be the dominant force. The bead should also rotate fast enough such that the perpendicular forces cause negligible translational motion. In general, the microswimmers will be controllable if they satisfy these conditions. In the ideal case, the perpendicular component of the propulsive force is zero so that at every time *t* the bead is instantaneously moving at a fixed speed in the commanded direction, **B**. The worst case is $F_p = F_p^{\perp}$, which will result in a circular motion with no net displacement. In most cases, the microswimmer will fall between these extremes and will trace out a helix (Figure 2c).

Characterization of one-dimensional steering control

We analyzed the trajectories of 35 microswimmers that displayed a persistent motion parallel or anti-parallel to the direction of the applied field when subjected to a constant

magnetic field of 10 mT (see Supplementary Movies 1, 2). Each microswimmer had about 1 to 10 attached bacterial cells, with the majority of the microswimmers containing about 5 - 6 bacterial cells (see Supplementary Fig. 2a for a probability distribution plot of bacterial attachment number). Representative trajectories of these samples are shown in Figure 3. As expected, the motion of the beads is strongly biased along the field direction. An oscillatory motion is also evident in the 2-D projection of the trajectories, which is indicative of a helical motion in 3-D (Figure 3b). Although all the tested beads showed a directional bias (i.e. their primary direction of motion was parallel to the applied field), the amplitude of the oscillations varied between samples. Figure 3c shows trajectories from three beads acquired over a 2-minute period. The first trajectory has much larger oscillations than the second and third trajectory, suggesting either a larger angle between the net propulsive force vector and the magnetic moment of the bead or a slower rotation rate about the magnetization axis. Upon removal of the magnetic field, the motion of the beads is no longer directional. Instead, it becomes stochastic, as shown in the fourth trajectory of Figure 3c. The significant difference between the third and fourth trajectories, which were produced by the same bead with and without an applied field, reveals the significant enhancement in bead controllability with the application of a uniform magnetic field.

The varying lengths of the trajectories in Figure 3c indicate a difference in the mean speed of the microswimmers. The mean instantaneous (2-D) speeds of the microswimmers ranged from 1.2 μm/s to 7.3 μm/s, which corresponds to applied propulsive forces ranging from 0.5 pN to 3.0 pN assuming Stokes flow ($\mathbf{F}_d = 6\pi\mu R_b\mathbf{v}$). The average (2-D) speed of all 35 beads was measured to be 2.4 ± 1.5 μm/s over a 30 s time interval. The microswimmers were shown to maintain their motility for at least 2 hours. To confirm that the microswimmer

motion is dominated by bacteria propulsion rather than a magnetic force, the mean instantaneous 2-D speeds of 30 microswimmers were compared when no magnetic field was applied and when a 10 mT field strength was applied. Although the directionality of the motion varied, no significant difference in the instantaneous speed was found before and after the application of the magnetic field (-3.9 ± 6.3% change with 95% confidence), confirming the bacteria-driven propulsion.

To characterize the controllability of the microswimmers, we computed the heading deviation angle, $\theta(\Delta t)$, defined as the angle between **B** and the average velocity, **v**, over an interval Δt

$$\theta(\Delta t) = \cos^{-1}\left(\frac{\mathbf{v}(\Delta t)\cdot\mathbf{B}}{|\mathbf{v}(\Delta t)||\mathbf{B}|}\right) \qquad (4)$$

The heading deviation angles are plotted in Figure 3d for the samples shown in Figure 3c. The solid red curve represents the root-mean-square heading deviation angle, θ_{RMS}, and the error bars denote the standard deviation, σ_θ. The root-mean-square heading is a measure of the directionality of the bead's motion over a given Δt, and the standard deviation is a measure of the oscillations in the motion over a given Δt. The shaded gray region ($\theta < 20^\circ$) corresponds to a high degree of steering control. For samples that are highly controllable (e.g. second and third plots), there is a significant decrease in the standard deviation as Δt increases, and θ converges to a mean value close to zero. The heading deviation angle results of the 35 analyzed samples are summarized in Figure 4, where σ_θ is plotted against θ_{RMS} for different time intervals. There is a significant decrease in both σ_θ and θ_{RMS} as Δt increases, indicating that the directional bias of the motion improves over longer time intervals. A small subset of these samples (35%) demonstrates a high degree of controllability ($\sigma_\theta < 20^\circ$ and $\theta_{RMS} < 20^\circ$) even over a short interval of 5 seconds.

Effect of bacterial attachment density and field strength on speed and controllability

An important assumption in the controllability of the microswimmers is that the bacterial propulsive torque does not exceed the maximum magnetic torque that can be applied on the bead. This assumption may not hold for lower field strengths or for higher bacteria attachment densities. In the previous controllability analyses, the bacterial attachment density was limited to about 10 bacteria per bead, and the applied field strength was 10 mT. Under these conditions, 87% of tested beads (N = 38) were found to be controllable (i.e. the magnetic moment of the beads remained aligned with the applied magnetic field). Controllable bead samples tended to have lower bacterial attachment numbers than uncontrollable bead samples as shown in Supplementary Fig. 2. If the bacterial attachment density is increased or the magnetic field strength is lowered, the probability that the bacterial propulsive torque will exceed the magnetic torque increases, thereby reducing the percentage of controllable beads.

The average speed of the microswimmers is also dependent on the number of attached bacterial cells as shown in Figure 5. The 2-D swimming speed was analyzed over a 15 second duration for 43 controllable samples. The swimming speed is shown to increase with the bacterial attachment density. Therefore, increasing the number of attached bacterial cells can improve the speed of the microswimmer. However, this increase in the attachment number can also increase the magnitude of the applied bacterial propulsive torque, which can negatively affect the controllability of the microswimmer if the propulsive torque exceeds the magnetic torque. The location and orientation of the bacterial cells on the bead can also

impact the speed and controllability of the microswimmer; however, these parameters were not quantified in this study.

Two-dimensional steering control

Steering the bacteria-propelled microbeads along complex paths requires rotation of the magnetic field; however, rotating the magnetic field too quickly can have detrimental effects on controllability. For example, superparamagnetic beads can remagnetize parallel or anti-parallel to their preferred axis of alignment (i.e. the easy axis) since they are soft magnets. If a constant field is applied such that the microswimmer is moving in the commanding direction and then the direction of the field is switched 180° instantaneously, no torque will be induced on the bead because it will simply remagnetize in the opposite direction (i.e. $\tau_m = 0$ since **m** and **B** are still parallel). Since the bead does not rotate, the velocity vector will remain in the same direction, and the microswimmer will not change its swimming direction. This phenomenon (i.e. no change in the swimming direction after an instantaneous 180° switch in magnetic field direction) was observed for the majority of microswimmers (93% of 22 tested samples). In contrast, if the field was slowly rotated 180°, a magnetic torque will be generated, and the microswimmer's velocity vector will rotate with the field.

To further analyze the effect of the field rotation rate on the steering controllability, we rotated the magnetic field 180° at frequencies ranging from 0.1 to 10 Hz and observed the microswimmer's turning motion. The magnetic field was rotated in increments of 45° since this angle produces the maximum magnetic torque (see equation 1). For cases where the bacteria-propelled microswimmer completed the 180° degree turn and started moving in the opposite direction, the turn was defined as a success. The results are shown in Figure 6a. The

turning success rate increased for lower rotational frequencies of the magnetic field. It was greater than 80% for field frequencies less than 0.5 Hz. To achieve a smaller turning radius, the field frequency should be maximized but remain below this critical frequency. By following this criterion, the bio-hybrid microswimmers can be steered along complex 2-D paths. Figure 6b shows the trajectory of a microswimmer that was steered to spell "CMU" under open-loop control (Supplementary Movie 4). Steering along square paths has also been demonstrated (Supplementary Movie 3). As shown, the microswimmers can be sufficiently steered using open-loop control, which may be acceptable for most applications. Closed-loop control with visual feedback may further enhance the steering precision. 3-D path following can also be achieved by integrating additional electromagnets into the system.

Discussion

We have demonstrated 1-D and 2-D magnetic steering control of bacteria-propelled microswimmers. The steering controllability of beads with randomly attached bacteria was characterized, and a set of controllability conditions for these microswimmers has been proposed. Optimizing the controllability of the microswimmers was not the goal of this study; however, we developed a model of the microswimmer's motion that can be used in future work to optimize the magnetic steering control. For practical applications, the microswimmers can be filtered based on their degree of steering controllability. Since the microswimmers have been observed to move parallel or anti-parallel to the applied field depending on the orientation of their net propulsive force vector with respect to the magnetic moment of the bead, it is critical to assess their direction of motion with respect to the polarity of the magnetic field before conducting a path following task. To control multiple microswimmers, a constant field can be applied to sort the swimmers into two groups: those

that move parallel to the field and those that move anti-parallel to the field. Then, each group of microswimmers can be steered as a unit. The concentration of the microswimmers should be kept low enough to limit bead-bead interactions, which could negatively affect the microswimmer controllability.

A number of paths towards optimizing the design of these bio-hybrid microswimmers are open. For example, although a random attachment of bacterial cells can produce controllable beads, the speed of the microswimmers can be increased by utilizing patterning techniques to attach the cells at specific sites on the bead and thus align the propulsive force vector with the magnetic moment of the bead. An improved alignment of the propulsive force vector with the magnetic moment of the bead will also reduce the amplitude of the oscillations in their motion. Alternate magnetic substrate geometries that minimize the drag force can also be explored.

In contrast to non-biological methods that rely on toxic fuels for actuation (e.g. hydrogen peroxide) or on large magnetic field strengths when magnetically-actuated with field gradients,[53] our bio-hybrid microswimmers can operate in biological media using low field strengths ($\leq$ 10 mT). Some previously developed magnetic non-biological microswimmers are also capable of propulsion with low field strengths, but require a continuously rotating or oscillating magnetic field for actuation.[30,32,54] Our microswimmers, in contrast, are actuated by the bacteria and only require a uniform magnetic field for steering control. The swimming speeds of our microswimmers are comparable to other bio-hybrid microdevices (~ 1 body length per second),[3] but they are slower than non-biological microswimmers, such as magnetic helical swimmers and micro-jet swimmers, which can achieve speeds greater than 10 body lengths per second.[25,32] The longest dimension of our

device is more than 5 times smaller than the spermatozoid-driven micro-tubes developed by Magdanz *et al.*, enabling navigation through tighter passages.[41]

For some applications, it might be advantageous to control a network or swarm of microswimmers to enable the parallel and distributed operation of tasks. For example, in drug delivery tasks, a swarm of microswimmers can deliver a greater volume of therapeutic agents than what could be carried by a single microdevice. To implement swarm control, however, advanced control methods are necessary. Since all the microswimmers within a workspace respond similarly to a uniform magnetic field, either moving parallel or anti-parallel to the direction of the applied field, navigating to a single target location using uniform fields is challenging. Advanced control strategies, such as the recently developed magnetic methods for aggregating magnetotactic bacteria,[37] or the integration of multiple control methods, such as combined external steering and sensory-based control, could be applied towards this goal. We can also make use of the properties of the superparamagnetic beads. When a magnetic field is applied, the microswimmers tend to be attracted to one another when in close proximity and form long chains along magnetic field lines. These interactions only persist under the presence of a field. Therefore, a large aggregate of microswimmers could be assembled and disassembled upon application and removal of a magnetic field, respectively. A small aggregate of microswimmers could be magnetically steered as a single unit as long as the bacterial propulsive force is large enough to maintain the motility.

One of the greatest advantages of bio-hybrid, magnetically steered microswimmers is that the bacteria's sensory response to external stimuli enables sensory-based steering control in addition to the external magnetic control. Sensory-based steering of *S. marcescens* using chemical signals has been demonstrated in previous work,[15,18,23] and the chemotactic control

and tumor targeting ability of bacterial species, such as *Salmonella typhimurium*, have been demonstrated.[21] As shown in Figure 7, we envision that remote, external steering can be combined with sensory-based control for search and targeted delivery tasks. For example, magnetic steering can be applied to navigate a microswimmer to a region of interest; then, the sensory-driven steering mechanisms can be engaged to move toward a target, such as the source of a biochemical signal in an *in vitro* bioanalysis device (Figure 7a). Another potential application is the use of externally driven and sensory-based steering simultaneously to control a swarm of microswimmers (Figure 7b). A single "leader" microswimmer can be magnetically steered and can guide a swarm of non-magnetic bacteria-propelled agents by releasing a chemoattractant signal, similar to the guide robot technique proposed by Nogawa *et al.*[55]

Conclusion

Our demonstrated externally driven magnetic control of individual, isolated microswimmers is a step towards controlling a swarm of bio-hybrid microswimmers. In future work, sensory-based steering methods can be integrated with the externally driven steering method proposed in this work, which could lead to novel control strategies for applications, such as localized drug delivery, lab-on-a-chip bioanalysis devices, and environmental monitoring. By introducing new control strategies for steering a large number of bio-hybrid microdevices, we open up new avenues for exploring the parallel and distributed operation of tasks in microscale environments.

Acknowledgements. We thank H. Teng for her assistance with the confocal imaging, M. J. Patrick for his advice on fluorescent staining, and S. Oberdick for obtaining the magnetometer measurements. We also thank E. Diller, J. Giltinan, and Z. Ye for their discussions, and Y. Gu and A. Veerubhotla for their experimental assistance. This work was supported by the National Science Foundation (NSF) Cyber Physical Systems Program (CNS-1135850) and an NSF Graduate Research Fellowship (Grant No. 09468251).

References

1. M. Sitti, Miniature devices: Voyage of the microrobots, *Nature*, 2009, **458**(7242), 1121-1122.

2. E. Diller and M. Sitti, Micro-Scale Mobile Robotics, *Found. Trends Databases*, 2013, **2**(3), 143-259.

3. V. Chan, H. Asada, and R. Bashir, Utilization and control of bioactuators across multiple length scales, *Lab Chip*, 2014, **14**, 653-670**.**

4. J. Kim, J. Park, S. Yang, J. Baek, B. Kim. S. H. Lee, E. Yoon, K. Chun and S. Park, Establishment of a fabrication method for a long-term actuated hybrid cell robot, *Lab Chip*, 2007, **7**(11), 1504-1508.

5. J. Xi, J. J. Schmidt and C. D. Montemagno, Self-assembled microdevices driven by muscle, *Nature Mater.*, 2005, **4**(2), 180-184.

6. A. W. Feinberg, A. Feigel, S. S. Shevkoplyas, S. Sheehy, G. M. Whitesides and K. K. Parker, Muscular thin films for buidling actuators and powering devices, *Science*, 2007, **317**(5843), 1366-1370.

7. B. J. Williams, S. V. Anand, J. Rajagopalan and M. T. A. Saif, A self-propelled biohybrid swimmer at low Reynolds number, *Nat. Commun.,* 2014, **5**,3081, DOI: 10.1038/ncomms4081.

8. B. Behkam and M. Sitti, Bacterial flagella-based propulsion and on/off motion control of microscale objects, *Appl. Phys. Lett.*, 2007, **90**(2), 023902.

9. M. Edwards, R. W. Carlsen and M. Sitti, Near and far-wall effects on the three-dimensional motion of bacteria-driven microbeads, *Appl. Phys. Lett.*, 2013, **102**(14), 143701.

10. R. Fernandes, M. Zuniga, F. R. Sassine, M. Karakoy and D. H. Gracias, Enabling Cargo-Carrying Bacteria via Surface Attachment and Triggered Release, *Small*, 2011, **7**(5), 588–592.

11. Q. Ma, C. Chen, S. Wei, C. Chen, L. Wu and T. Song, Construction and operation of a microrobot based on magnetotactic bacteria in a microfluidic chip, *Biomicrofluidics*, 2012, **6**(2), 024107.

12. S. J. Park, H. Bae, J. Kim, B. Lim, J. Park and S. Park, Motility enhancement of bacteria actuated microstructures using selective bacteria adhesion, *Lab Chip*, 2010, **10**(13), 1706-1711.

13. M. S. Sakar, E. B. Steager, D. H. Kim, A. A. Julius, M. J. Kim, V. Kumar and G. J. Pappas, Modeling, control and experimental characterization of microbiorobots, *Int. J. Robot. Res.*, 2011, **30**(6), 647-658.

14. T. Tran, D. H. Kim, J. Kim, M. J. Kim and D. Byun, Use of an AC electric field in galvanotactic on/off switching of the motion of a microstructure blotted by *Serratia marcescens*, *Appl. Phys. Lett.*, 2011, **99**(6), 063702.

15. M. A. Traoré, A. Sahari and B. Behkam, Computational and experimental study of chemotaxis of an ensemble of bacteria attached to a microbead, *Phys. Rev. E*, 2011, **84** (6), 061908.

16. E. B. Steager, M. S. Sakar, D. H. Kim, V. Kumar, G. J. Pappas and M. J. Kim, Electrokinetic and optical control of bacterial microrobots, *J. Micromech. Microeng.*, 2011, **21**(3), 035001.

17. S. J. Park, H. Bae, S. Y. Ko, J. Min, J. Park and S. Park, Selective bacterial patterning using the submerged properties of microbeads on agarose gel, *Biomed. Microdevices*, 2013, **15**(5), 793-799.

18. D. Kim, A. Liu, E. Diller and M. Sitti, Chemotactic steering of bacteria propelled microbeads, *Biomed. Microdevices*, 2012, **14** (6), 1009-1017.

19. M. Kojima, Z. Zhang, M. Nakajima, K. Ooe and T. Fukuda, Construction and evaluation of bacteria-driven liposome, *Sensors Actuat. B-Chem.*, 2013, **183**, 395–400.

20. S. Martel, Bacterial microsystems and microrobots, *Biomed. Microdevices*, 2012, **14**(6), 1033-1045.

21. S. J. Park, S. Park, S. Cho, D. Kim, Y. Lee, S. Y. Ko, Y. Hong, H. E. Choy, J. Min, J. Park and S. Park, New paradigm for tumor theranostic methodology using bacteria-based

microrobot, *Sci. Rep.*, 2013, **3**, 3394, DOI:10.1038/srep03394.

22. M. A. Traore and B. Behkam, A stochastic model for chemotactic motion of micro-beads propelled by attached bacteria, In *Biomed. Robot. Biomechatron. (BioRob), 2010 3rd IEEE RAS and EMBS International Conference,* IEEE, 2010, 704-709.

23. D. Park, S. J. Park, S. Cho, Y. Lee, Y. K. Lee, J. Min, B. J. Park, S. Y. Ko, J. Park and S. Park, Motility analysis of bacteria-based microrobot (bacteriobot) using chemical gradient microchamber, *Biotech. Bioeng.*, 2014, **111**(1), 134-143.

24. R. S. M. Rikken, R. J. M. Nolte, J. C. Maan, J. C. M. van Hest, D. A. Wilson and P. C. M. Christianen, Manipulation of micro- and nanostructure motion with magnetic fields, *Soft Matter*, 2014, **10**, 1295-1308.

25. I. S. M. Khalil, V. Magdanz, S. Sanchez, O. G. Schmidt and S. Misra, Three-dimensional closed-loop control of self-propelled microjets, *Appl. Phys. Lett.*, 2013, **103**(17), 172404.

26. H. Choi, J. Choi, G. Jang, J. Park and S. Park, Two-dimensional actuation of a microrobot with a stationary two-pair coil system, *Smart Mater. Struct.*, 2009, **18**(5), 055007.

27. K. B. Yesin, K. Vollmers and B. J. Nelson, Modeling and control of untethered biomicrorobots in a fluidic environment using electromagnetic fields, *Int. J. Robot. Res.*, 2006, **25**(5-6), 527-536.

28. M. S. Sakar, E. B. Steager, D. H. Kim, M. J. Kim, G. J. Pappas and V. Kumar, Single cell manipulation using ferromagnetic composite microtransporters, *Appl. Phys. Lett.*, 2010, **96**(4), 043705.

29. A. A. Solovev, S. Sanchez, M. Pumera, Y. F. Mei and O. G. Schmidt, Magnetic control of tubular catalytic microrobots for the transport, assembly, and delivery of micro-objects, *Adv. Funct. Mater.*, 2010, **20**, 2430-2435.

30. L. Zhang, K. E. Peyer and B. J. Nelson, Artificial bacterial flagella for micromanipulation, *Lab Chip*, 2010, **10**(17), 2203-2215.

31. A. Ghosh and P. Fischer, Controlled propulsion of artificial magnetic nanostructured propellers, *Nano Lett.*, 2009, **9**(6), 2243–2245.

32. S. Tottori, L. Zhang, F. Qiu, K. K. Krawczyk, A. Franco-Obregon and B. J. Nelson, Magnetic helical micromachines: fabrication, controlled swimming, and cargo transport, *Adv. Mater.*, 2012, **24**(6), 811-816.

33. S. Kim, F. Qiu, S. Kim, A. Ghanbari, C. Moon, L. Zhang, B. J. Nelson and H. Choi, Fabrication and characterization of magnetic microrobots for three-dimensional cell culture and targeted transportation, *Adv. Mater.*, 2013, **25**(41), 5863–5868.

34. J. Li, S. Sattayasamitsathit, R. Dong, W. Gao, R. Tam, X. Feng, S. Ai and J. Wang,

Template electrosynthesis of tailored-made helical nanoswimmers, *Nanoscale*, 2014, DOI: 10.1039/c3nr04760a.

35. S. Martel, M. Mohammadi, O. Felfoul, Z. Lu and P. Pouponneau, Flagellated magnetotactic bacteria as controlled MRI-trackable propulsion and steering systems for medical nanorobots operating in the human microvasculature, *Int. J. Robot. Res.*, 2009, **28**(4), 571-582.

36. H. Lee, H., A. M. Purdon, V. Chu and R. M. Westervelt, Controlled assembly of magnetic nanoparticles from magnetotactic bacteria using microelectromagnets arrays, *Nano Lett.*, 2004, **4**(5), 995–998.

37. D. de Lanauze, O. Felfoul, J. P. Turcot, M. Mohammadi and S. Martel, Three-dimensional remote aggregation and steering of magnetotactic bacteria microrobots for drug delivery applications, *Int. J. Robot. Res.*, 2013, DOI: 10.1177/0278364913500543.

38. I. S. M. Khalil, M. P. Pichel, L. Zondervan, L. Abelmann and S. Misra, Characterization and control of biological microrobots, *Experimental Robotics*, 2013, **88**, 617-631.

39. O. Felfoul and S. Martel, Assessment of navigation control strategy for magnetotactic bacteria in microchannel: toward targeting solid tumors, *Biomed. Microdevices*, 2013, **15**(6), 1015-1024.

40. Y. Ou, D. H. Kim, P. Kim, M. J. Kim and A. A. Julius, Motion control of magnetized *Tetrahymena pyriformis* cells by a magnetic field with Model Predictive Control. *Int. J. Robot. Res.*, 2013, **32**(1), 129-139.

41. V. Magdanz, S. Sanchez and O. G. Schmidt, Development of a sperm-flagella driven micro-bio-robot, *Adv. Mater.*, 2013, **25**(45), 6581-6588.

42. A. Zita and M. Hermansson, Determination of bacterial cell surface hydrophobicity of single cells in cultures and in wasterwater in situ, *FEMS Microbiol. Lett.*, 1997, **152**(2), 299-306.

43. J. S. Dickson and M. Koohmaraie, Cell surface charge characteristics and their relationship to bacterial attachment to meat surfaces, *Appl. Environ. Microbiol.*, 1989, **55**(4), 832-836.

44. A. Hejazi and F. R. Falkiner, Serratia marcescens, *J. Med. Microbiol.*, 1997, **46**(11), 903-912.

45. N. Darnton, L. Turner, K. Breuer and H. C. Berg, Moving fluid with bacterial carpets, *Biophys. J.*, 2004, **86**(3), 1863–1870.

46. D. Wong, E. E. Beattie, E. B. Steager and V. Kumar, Effect of surface interactions and geometry on the motion of micro bio robots, *Appl. Phys. Lett.*, 2013, **103**(15), 153707.

47. M. R. Edwards, R. W. Carlsen, J. Zhuang and M. Sitti, Swimming characterization of *Serratia marcescens* for bio-hybrid micro-robotics, *J. Micro-Bio. Robot.*, 2014, **9**(3), 47-60.

48. B. Behkam and M. Sitti, Effect of quantity and configuration of attached bacteria on bacterial propulsion of microbeads, *Appl. Phys. Lett.*, 2008, **93**(22), 223901.

49. E. B. Wilson, Probable inference, the law of succession, and statistical inference, *J. Am. Statist. Assoc.*, 1927, **22**(158), 209-212.

50. D. Klaue and R. Seidel, Torsional stiffness of single superparamagnetic microspheres in an external magnetic field, *Phys. Rev. Lett.*, 2009, **102**(2), 028302.

51. K. C. Neuman, T. Lionnet and J. F. Allemand, Single-molecule micromanipulation techniques, *Ann. Rev. Mater. Res.*, 2007, **37**, 33-67.

52. F. Mosconi, J. F. Allemand and V. Croquette, Soft magnetic tweezers: A proof of principle, *Rev. Sci. Instrum.*, 2011, **82**(3), 032302.

53. L. K. Abdelmohsen, F. Peng, Y. Tu, D. A. Wilson, Micro-and nano-motors for biomedical applications, *J. Mater. Chem. B.*, 2014, **2**, 2395-2408.

54. R. Dreyfus, J. Baudry, M. L. Roper, M. Fermigier, H. A. Stone and J. Bibette, Microscopic artificial swimmers, *Nature*, 2005, **437**(7060), 862-865.

55. K. Nogawa, M. Kojima, M. Nakajima, M. Homma, F. Arai and T. Fukuda, Smart manipulation of multiple bacteria-driven microobjects based on bacterial autonomous movement, In *Intelligent Robots and Systems (IROS), 2011 IEEE/RSJ International Conference*, IEEE, 2011, 1693-1698.

Figure Legends and Tables:

Figure 1. **Magnetic coil system.** (a) A uniform magnetic field is generated by four orthogonally oriented iron-core electromagnets, which are built into a microscope stage insert. (b) The workspace between the coils is 36 mm x 36 mm. (c) The coils are connected to a 24 V and 20 A power supply. (d) The coil current is controlled with an Arduino Uno microcontroller board (http://www.arduino.cc). (e) The samples are imaged using a 32x objective in an inverted phase contrast microscope (Zeiss Axio Observer). (f) Images of the microbeads were captured at 20 frames per second with a QICAM digital camera (QImaging).

Figure 2. **Magnetically steered, bacteria-propelled microbead.** (a) If the bead's easy axis is not initially aligned with an applied field **B**, a magnetic torque ($\boldsymbol{\tau}_m = \mathbf{m}_{\parallel} \times \mathbf{B}$) is produced that induces a rotation of the bead. (b) When bacteria are attached to the bead, they generate a net propulsive force $\mathbf{F}_p$ and torque $\boldsymbol{\tau}_p$. The components of these forces and torques are shown, where $\mathbf{F}_p^{\parallel}$ and $\boldsymbol{\tau}_p^{\parallel}$ are defined as the components parallel to the bead's easy axis, and $\mathbf{F}_p^{\perp}$ and $\boldsymbol{\tau}_p^{\perp}$ are the components perpendicular to the easy axis. (c) The relationship between the net propulsive force $\mathbf{F}_p$, the net propulsive torque $\boldsymbol{\tau}_p$, and the magnetic moment **m** of the bead dictates the motion of the microswimmer. If a uniform magnetic field is applied and $\tau_m \gg \tau_p^{\perp}$, the magnetic moment of the bead aligns with the applied field, and the bead is only free to rotate about its easy axis. The bead will move in a straight line if $\mathbf{F}_p$ is parallel to **m**. If $\mathbf{F}_p$ is perpendicular to **m**, a circular motion results. In general, $\mathbf{F}_p$ is between these two extremes, and the bead moves with velocity **v** in a helical path as shown.

Figure 3. **One-dimensional line following analysis.** (a) Time-lapse optical images (5 s interval) of a bacteria-propelled superparamagnetic microbead subjected to a uniform magnetic field (B_x = 10 mT). The solid red line indicates the bead's trajectory. Insets (i) and (ii) are confocal images of a single bacterial cell (*Serratia marcescens*) and of several cells attached to a microbead, respectively. The bacteria are labeled with Alexa Fluor 594 (Molecular Probes, Eugene, OR) and appear white in the images. Note: The confocal and optical images are from different bead samples. (b) A portion of the 2-D trajectory shown in (a) is plotted in 3-D, revealing the helical nature of the bead's trajectory. (c) Representative trajectories of microbeads subjected to a uniform 10 mT magnetic field (top three plots) and of a microbead subjected to no magnetic field (bottom plot). The third and fourth trajectories are from the same microbead, which demonstrates the effect of the magnetic field on the bead's motion. All the trajectories were obtained over a 2-minute period. (c) The corresponding heading deviation angle plots are shown for each trajectory in (b). The solid red curve indicates the root-mean-square heading, and the error bars represent the standard deviation. For the case where $\mathbf{B} = 0$, we assume a commanding heading in the x-direction. The heading deviation angle, θ, is a direct experimental measure of the bead's controllability. Smaller standard deviations and mean angles closer to zero (within the shaded gray region) correspond to better steering control. Scale bars: (a) 20 μm, (i) 5 μm, (ii) 10 μm.

Figure 4. **One-dimensional line following test results.** Thirty-five bacteria-propelled microbead samples were subjected to a uniform magnetic field (B_x = 10 mT). The heading deviation angles, θ, were computed for each sample at four different time intervals (Δt = 1, 5, 30, 60 s). Each marker represents the standard deviation and root-mean-square (RMS)

heading angle of a single sample for a given Δt. The shaded regions encompass all the points with the same Δt. Tighter steering control is achieved over a given time interval if the standard deviation and mean angle is closer to zero (towards the origin). Given the helical nature of the bead motion, the motion is fairly random at short times, but the directionality of the motion improves over longer time intervals. This is evident by the decrease in the standard deviation and mean angle of all samples as Δt increases. The characteristic time scale over which a tight degree of control can be achieved varies from sample to sample; however, the samples can be evaluated as more controllable over longer Δt.

Figure 5. **Effect of bacterial attachment number on swimming speed.** The average 2-D swimming speed over a 15 second duration is plotted for microswimmers with different numbers of attached bacteria. A total of 43 controllable samples were analyzed. The error bars indicate the sample standard deviation.

Figure 6. **Two-dimensional steering control test results.** (a) The success rates to complete a 180° turn when the magnetic field is rotated at 45° increments at frequencies ranging from 0.1 to 10 Hz are shown. A total of 40 turns (2 turns from 20 bead samples) was analyzed for each turning rate. The error bars indicate a 95% binomial proportion confidence interval using a Wilson score[49]. The field frequency must be kept below 0.5 Hz to achieve turning success rates greater than 80%. (b) Using a pre-programmed control algorithm that varies the direction of the applied magnetic field (10 mT) with time, a microbead is steered to spell "CMU". Here, the rotational frequency of the magnetic field was kept below 0.25 Hz. The

trajectory took 1.5 minutes to complete. The bead positions are shown every 5 seconds, and the inset shows the desired trajectory. Scale bar: 20 μm.

Figure 7. **Future direction of integrating passive and active control of bacteria-propelled microswimmers.** (a) A microswimmer is externally steered (e.g. using magnetic fields) towards the sensory-based control region, where the external steering is removed and sensory-based steering (e.g. chemotactic control) is engaged to navigate towards a target site (e.g. chemical source). (b) The leading microswimmer is magnetically steered and releases a chemical signal to guide the other non-magnetic swarm agents.

Table 1. **Conditions for bio-hybrid microswimmer controllability.**

Table 1.

Condition	Description
$\frac{\langle F_p' \rangle_t}{\bar{F}_p} \ll 1$	The fluctuations in the propulsive force must be small compared to its mean value over a characteristic time
$\frac{\langle \tau_p' \rangle_t}{\bar{\tau}_p} \ll 1$	The fluctuations in the propulsive torque must be small compared to its mean value over a characteristic time
$\frac{\tau_p^{\perp}}{\tau_m^{\max}} \ll 1$	The propulsive torque perpendicular to the commanded direction must be small compared to the applied magnetic torque
$\frac{F_p^{\perp}}{\tau_p^{\parallel}} < 1$	The bead must rotate quickly compared to the speed at which it translates perpendicular to the commanded direction
$\frac{F_p^{\perp}}{F_p^{\parallel}} < 1$	The propulsive force in the commanded direction must not be small compared to the force perpendicular to it
$\frac{F_p^{\parallel}}{F_{\text{other}}} \gg 1$	The propulsive force is the dominant force acting on the bead

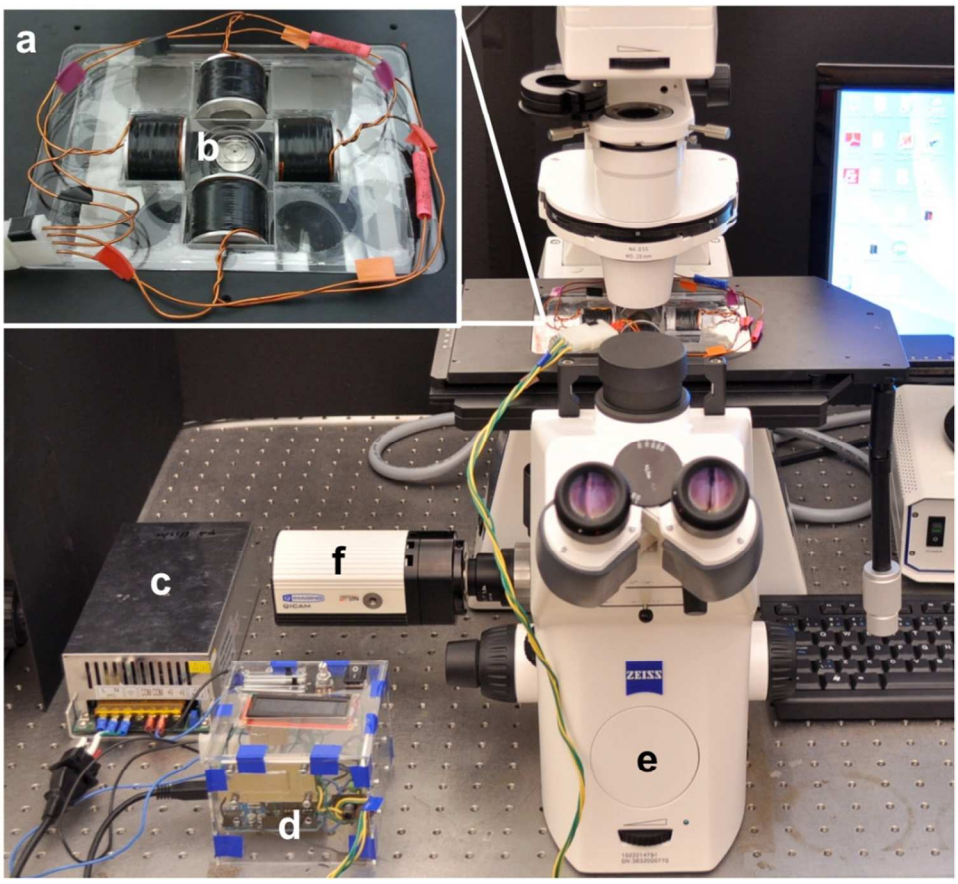

Figure 1

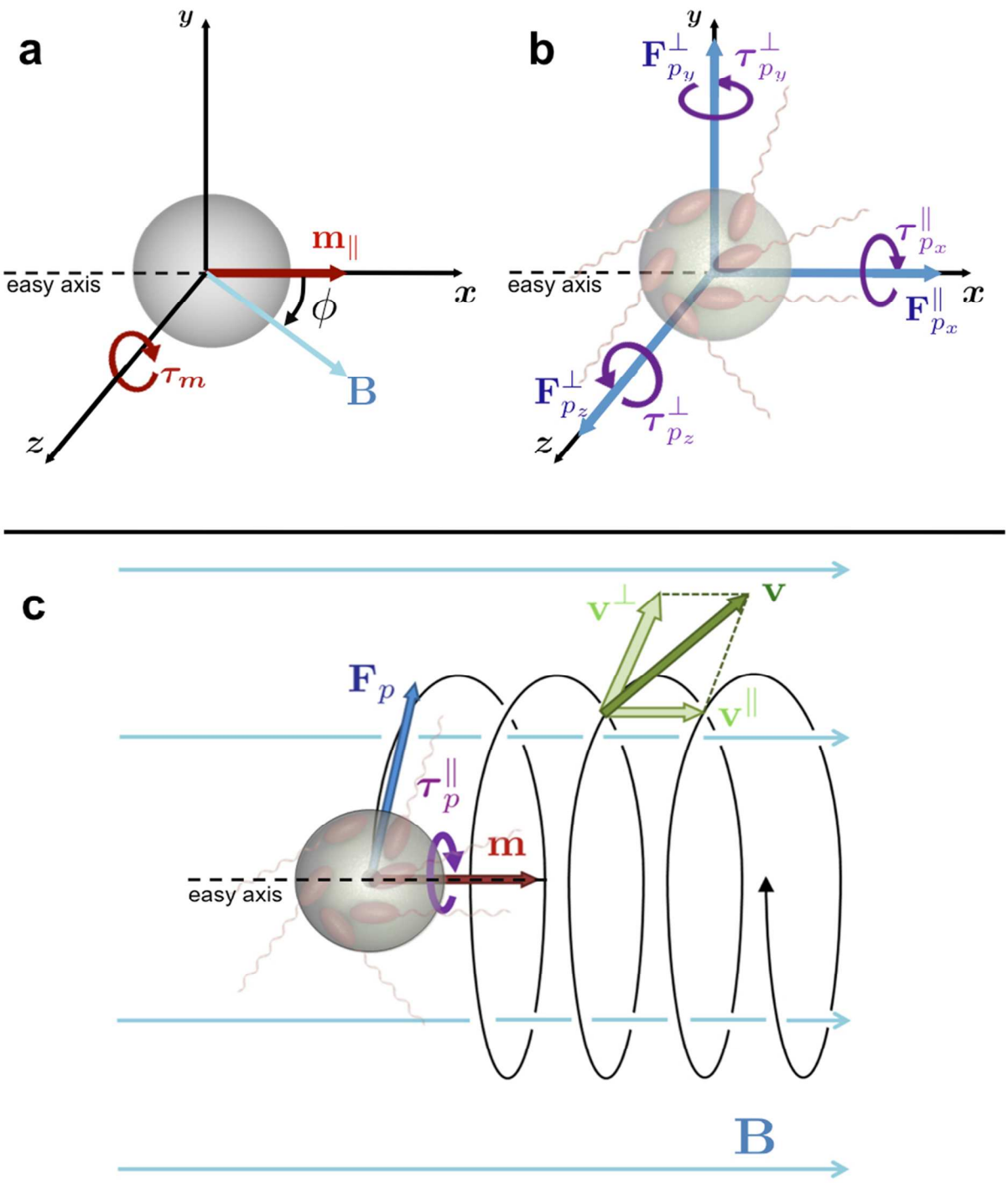

Figure 2

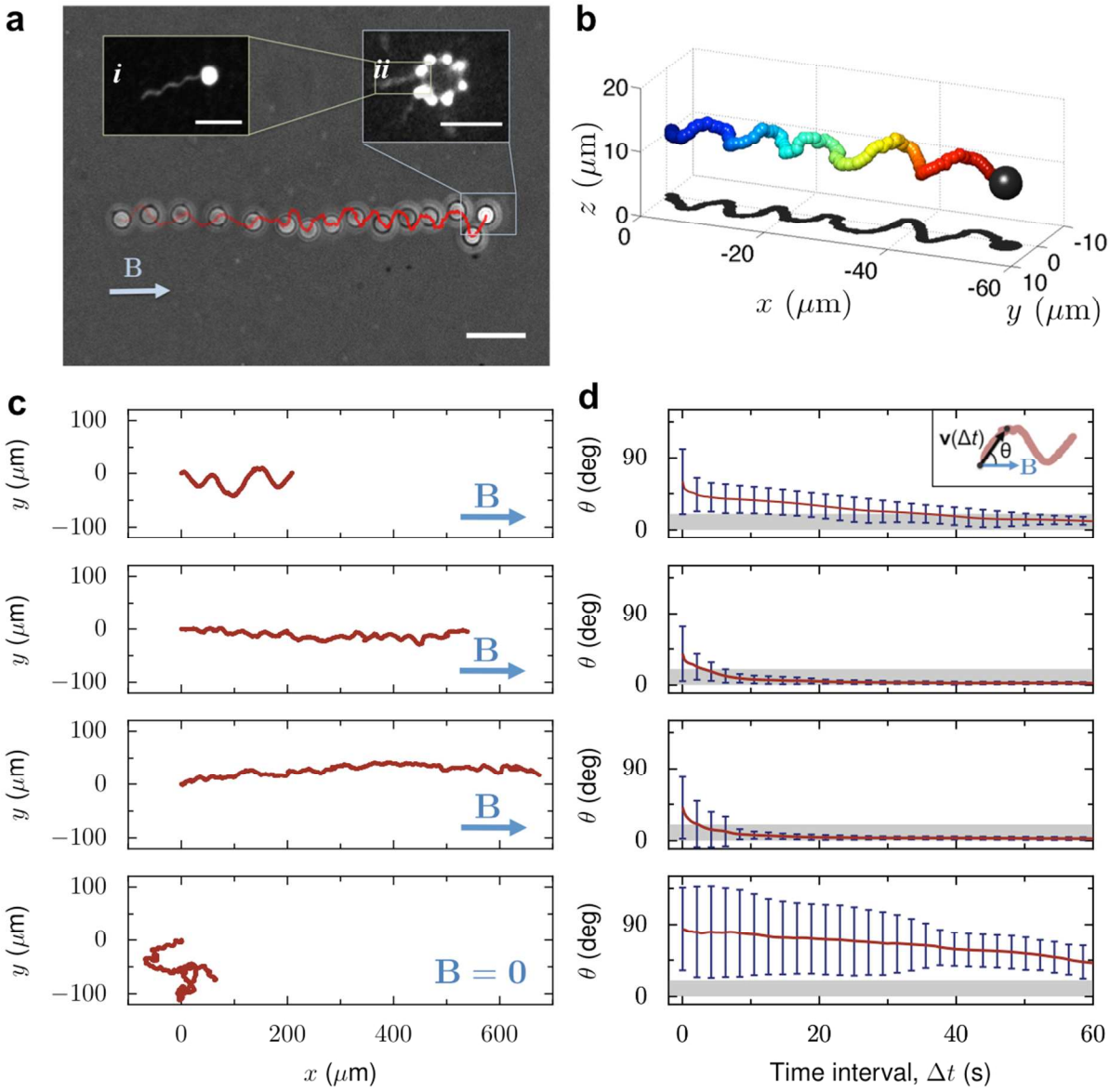

Figure 3

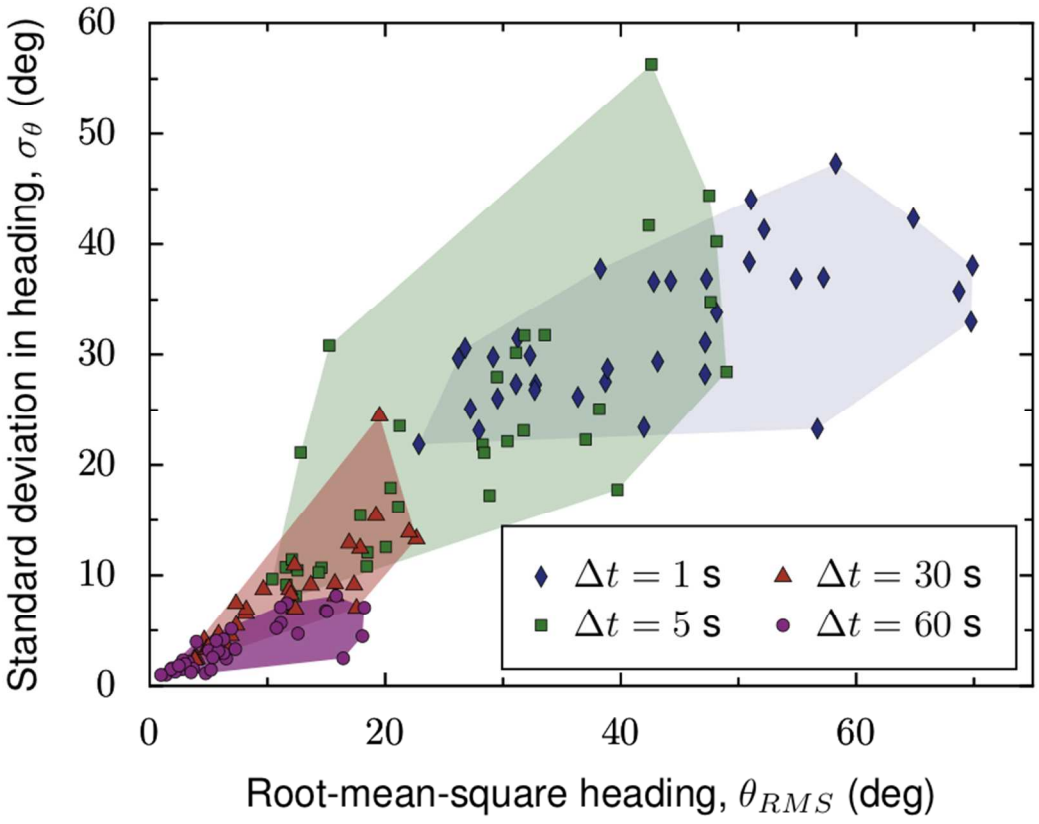

Figure 4

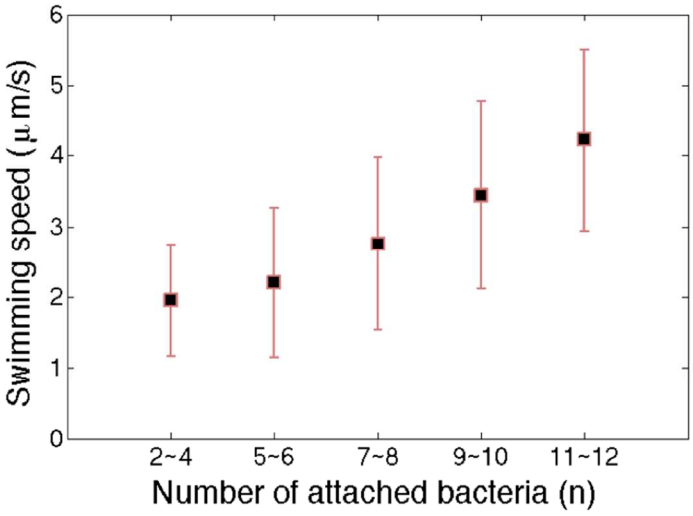

Figure 5

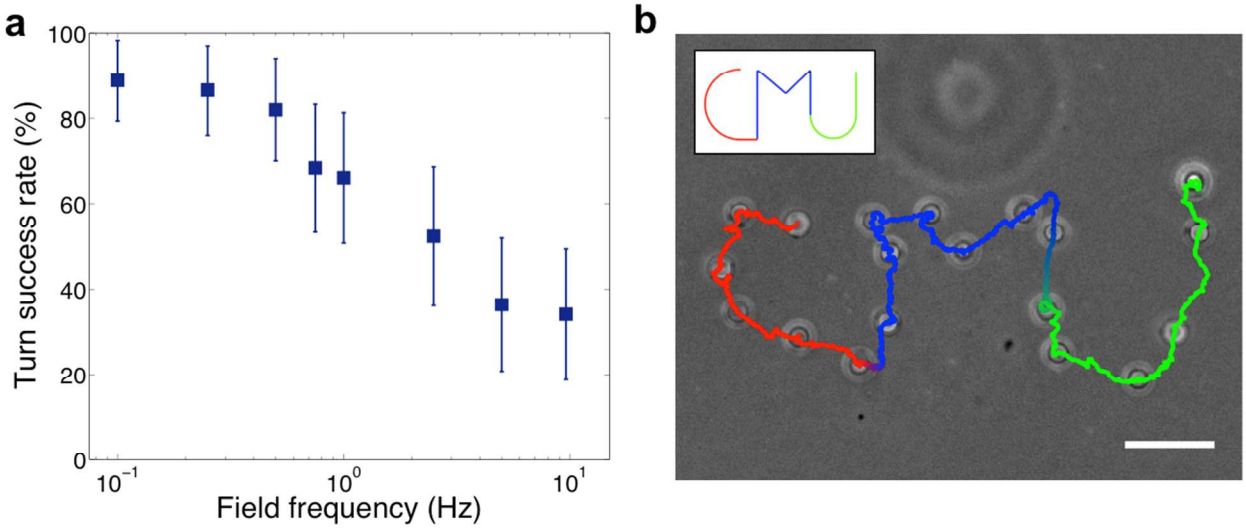

Figure 6

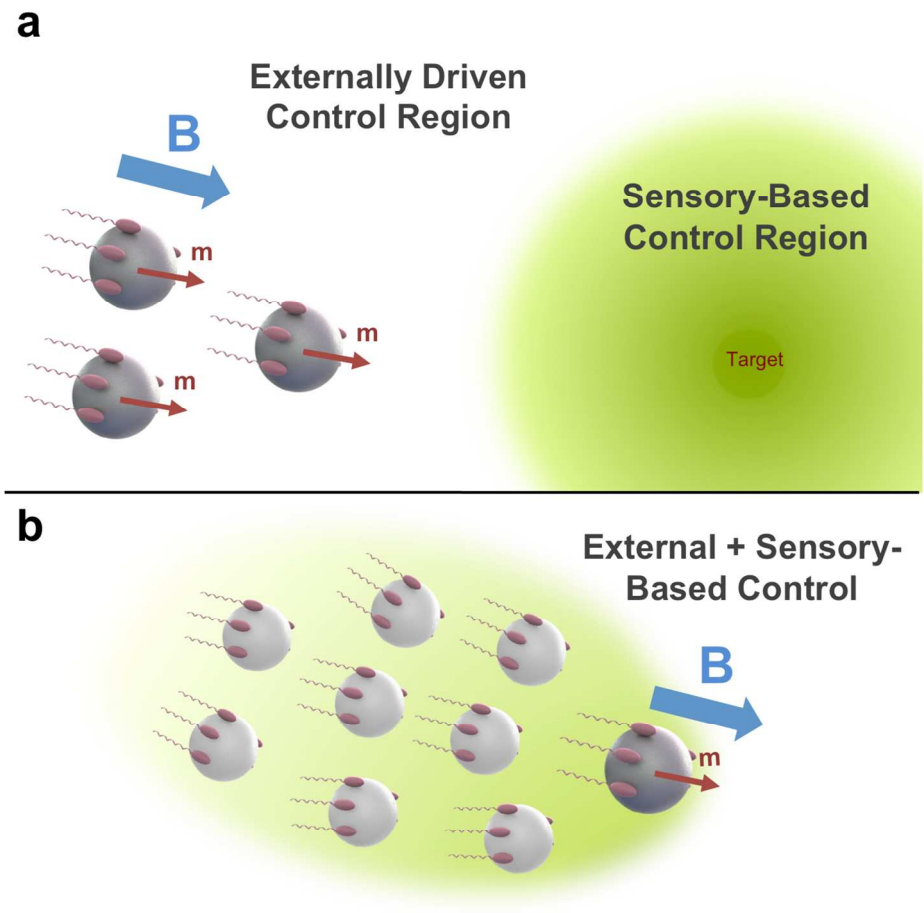

Figure 7